Environmental Pollution 233 (2018) 1086–1094

Contents lists available at ScienceDirect

Environmental Pollution

journal homepage: www.elsevier.com/locate/envpol

Estimating spatiotemporal distribution of PM_1 concentrations in China with satellite remote sensing, meteorology, and land use information☆

Gongbo Chen [a], Luke D. Knibbs [b], Wenyi Zhang [c], Shanshan Li [a], Wei Cao [d], Jianping Guo [e], Hongyan Ren [d], Boguang Wang [f], Hao Wang [g], Gail Williams [b], N.A.S. Hamm [h], Yuming Guo [a, *]

[a] Department of Epidemiology and Preventive Medicine, School of Public Health and Preventive Medicine, Monash University, Melbourne, Australia
[b] School of Public Health, The University of Queensland, Brisbane, Australia
[c] Center for Disease Surveillance & Research, Institute of Disease Control and Prevention, Academy of Military Medical Science, Beijing, China
[d] Institute of Geographic Sciences and Natural Resources Research, Chinese Academy of Sciences, Beijing, China
[e] Sate Key Laboratory of Severe Weather, Chinese Academy of Meteorological Sciences, Beijing, China
[f] Institute for Environmental and Climate Research, Jinan University, Guangzhou, China
[g] Air Quality Studies, Department of Civil and Environmental Engineering, Hong Kong Polytechnic University, Hong Kong, China
[h] Faculty of Geo-Information Science and Earth Observation (ITC), University of Twente, Enschede, The Netherlands

A R T I C L E I N F O

Article history:
Received 29 July 2017
Received in revised form
19 September 2017
Accepted 4 October 2017
Available online 13 October 2017

Keywords:
PM_1
Aerosol optical depth
Meteorology
Land use
China

A B S T R A C T

Background: PM_1 might be more hazardous than $PM_{2.5}$ (particulate matter with an aerodynamic diameter $\leq$ 1 μm and $\leq$2.5 μm, respectively). However, studies on PM_1 concentrations and its health effects are limited due to a lack of PM_1 monitoring data.
Objectives: To estimate spatial and temporal variations of PM_1 concentrations in China during 2005–2014 using satellite remote sensing, meteorology, and land use information.
Methods: Two types of Moderate Resolution Imaging Spectroradiometer (MODIS) Collection 6 aerosol optical depth (AOD) data, Dark Target (DT) and Deep Blue (DB), were combined. Generalised additive model (GAM) was developed to link ground-monitored PM_1 data with AOD data and other spatial and temporal predictors (e.g., urban cover, forest cover and calendar month). A 10-fold cross-validation was performed to assess the predictive ability.
Results: The results of 10-fold cross-validation showed R^2 and Root Mean Squared Error (RMSE) for monthly prediction were 71% and 13.0 μg/m^3, respectively. For seasonal prediction, the R^2 and RMSE were 77% and 11.4 μg/m^3, respectively. The predicted annual mean concentration of PM_1 across China was 26.9 μg/m^3. The PM_1 level was highest in winter while lowest in summer. Generally, the PM_1 levels in entire China did not substantially change during the past decade. Regarding local heavy polluted regions, PM_1 levels increased substantially in the South-Western Hebei and Beijing-Tianjin region.
Conclusions: GAM with satellite-retrieved AOD, meteorology, and land use information has high predictive ability to estimate ground-level PM_1. Ambient PM_1 reached high levels in China during the past decade. The estimated results can be applied to evaluate the health effects of PM_1.

1. Introduction

With the rapid growth of the economy and expansion of the urban population, China is experiencing serious air pollution problems causing 1.6 million deaths nationwide annually (Kan et al., 2009; Rohde and Muller, 2015). Fine particulate matter with aerodynamic diameter $\leq$2.5 μm ($PM_{2.5}$) has attracted increasing public concern and its adverse health effects have been documented by numerous studies (Cao et al., 2012; Dockery and Stone, 2007; Ma et al., 2011; Yang et al., 2012). Particulate matter with aerodynamic diameter $\leq$1 μm (PM_1), a major part of fine particulate matter mass, has seldom been studied – either to investigate its spatiotemporal variation or to investigate its associations with health outcomes. PM_1 accounts for more than 80% of

☆ This paper has been recommended for acceptance by B. Nowack.

* Corresponding author. Department of Epidemiology and Preventive Medicine, School of Public Health and Preventive Medicine, Monash University. Level 2, 553 St Kilda Road, Melbourne, VIC 3004, Australia.
E-mail address: yuming.guo@monash.edu (Y. Guo).

https://doi.org/10.1016/j.envpol.2017.10.011

ambient $PM_{2.5}$ mass at some locations, particularly in China (Cabada et al., 2004; Li et al., 2015; Wang et al., 2015). Due to its smaller particle size, PM_1 might be more harmful than $PM_{2.5}$ and more strongly associated with some health outcomes (Chen et al., 2017; Lin et al., 2016).

To fill in spatial and temporal gaps left by ground-based measurements of air pollution, satellite remote sensing has been used successfully in recent years to predict concentrations of air pollution at locations with sparse ground monitoring data, based on the validated relationships between satellite remote sensing and ground measurements (Hu et al., 2014b; Just et al., 2015; Kloog et al., 2012; Koelemeijer et al., 2006). Aerosol optical depth (AOD), also referred to as aerosol optical thickness (AOT), is the most widely used satellite-retrieved atmospheric product that has been used to predict air pollution concentrations. AOD is a measure of the attenuation of solar radiation by aerosols in the atmosphere and is correlated with PM concentration at ground level in many regions (Koelemeijer et al., 2006; Lee et al., 2011). Previous studies have reported satellite-retrieved concentrations of $PM_{2.5}$ and PM_{10} (particulate matter with aerodynamic diameter ≤ 10 μm) in China using AOD and other predictors with high spatial resolution and predictive ability (Fang et al., 2016; Ma et al., 2015; Meng et al., 2015; Zheng et al., 2016), but no study has reported satellite-retrieved concentrations of PM_1.

In this study, we aimed to combine daily ground monitoring data of PM_1 and Moderate Resolution Imaging Spectroradiometer (MODIS) Collection 6 AOD data with other spatial and temporal predictors to estimate the concentrations of PM_1 across China during 2005–2014.

2. Materials

2.1. Ground measurements of PM_1 and $PM_{2.5}$

Hourly ground-level measurements of PM_1 and $PM_{2.5}$ were obtained from 77 stations of China Atmosphere Watch Network (CAWNET) from November 2013 to July 2014 and September 2013 to December 2014, respectively (Guo et al., 2009, 2017). We used this time span because it had contemporaneous measurements of both particle sizes. Hourly concentrations of PM_1 and $PM_{2.5}$ during the study period were measured with the GRIMM 180 (Grimm 180 Multi-channel Aerosol Spectrometer) environmental dust monitors (Grimm and Eatough, 2009). This instrument is an optical particle counter (OPC) with 31 size channels and operates at a flow rate of 1.2 L/min. The recorded particle size number distribution between 0.25 μm and 32 μm is then calibrated to a particle mass concentration. Details about the measurements and calibration were reported previously (Wang et al., 2015). Daily mean concentrations of PM_1 and $PM_{2.5}$ were calculated as ($C_{daily} = \sum_1^{24} C_{hour}/24$), where C denotes the PM_1 or $PM_{2.5}$ concentrations. Two approaches were applied to control the quality of PM_1 measurements (Guo et al., 2009). The locations of 77 monitoring stations are shown in Fig. 1. More stations were located in Eastern and Central China, especially for South-Eastern coastal areas, than Western China.

2.2. Aerosol optical depth

Two types of daily MODIS AOD data, Dark Target (DT) and Deep Blue (DB), from the Aqua Atmosphere Level 2 Product Collection 6 at 10-km resolution and covering China were downloaded from NASA Level-1 and Atmosphere Archive & Distribution System Distributed Active Archive Centre for 2005 to 2014 (https://ladsweb.nascom.nasa.gov/search/index.html). DT and DB AOD were then combined with an Inverse Variance Weighting Method after filling the their gaps (Ma et al., 2015). A merged AOD product of DT AOD and DB AOD was available via NASA (MODIS Aerosols Merged Dark Target Deep Blue Product) in which DB AOD values were discarded with Normalized Difference Vegetation Index (NDVI) values greater than 0.3 (Levy et al., 2013). To increase the spatial coverage of AOD data, this merged product was not used in this study, we instead, obtained DT and DB AOD products separately and used the approach of Ma et al. (2015) to fill the missing values in both products and combine them (Ma et al., 2015). A model linking DT and DB AOD data was developed to fill the missing values. This model was based on simple linear regression:

$$AOD_{DT} = \alpha + \beta * AOD_{DB} + \varepsilon$$

where: AOD_{DT} is the DT AOD value; AOD_{DB} is the DB AOD value; α is the intercept and β is the slope coefficient and ε is a normally distributed residual. This model was used to fill the missing values of DT AOD when values of DB AOD were valid, and vice-versa. Ground-measured AOD data in China during the study period were downloaded from the Aerosol Robotic Network (AERONET) (https://aeronet.gsfc.nasa.gov/) to combine DT and DB AOD data. The AERONET AOD data at 675 nm and 440 nm were extracted to interpolate the AOD values at 550 nm, which were then linked with DT and DB AOD by location and time (Jing-Mei et al., 2010; Sayer et al., 2013). Details about the interpolation are shown in “Interpolation of AOD at 550 nm” in the Supplemental Material. The differences between DB AOD (or DT AOD) and AERONET AOD were calculated, and the inverse variances of these differences were used as weight to combine DB and DT AOD data. The locations of 40 AERONET sites providing ground-measured AOD data are shown in Fig. S1 in the Supplemental Material. Compared with merged AOD product available at Aqua MODIS C6, the combined AOD data derived using methods above showed a substantial improvement in spatial coverage (Ma et al., 2015).

2.3. Meteorological data

Daily meteorological data were obtained from 824 weather stations of the China meteorological data sharing service system during 2005–2014 (http://data.cma.gov.cn). The locations of these weather stations are shown in Fig. S2 in the Supplemental Material. Daily mean temperature, relative humidity, barometric pressure and wind speed were used in this study. Meteorological variables in areas not covered by weather stations were interpolated using “Micro krig” in the R package “fields” (Furrer et al., 2009). The details of this interpolation are shown in “Interpolation of meteorological variables” in the Supplemental Material.

2.4. Land use information and vegetation data

Annual land cover data (including urban cover, forest cover, and water cover) from 2004 to 2012 at a spatial resolution of 500 m were obtained from Global Mosaics of the standard MODIS land cover type data Collection 5.1 product of Global Land Cover Facility (http://glcf.umd.edu/) (Friedl et al., 2010). Land cover data in 2012 were used for prediction of study years 2012–2014, as the data were not available during 2013 and 2014. In total, there are 17 types of land cover variables in the satellite data sets and the pixel size is 500 m. The percentages of forest cover (or other types of land cover) were calculated by dividing the count of forest cover pixels by the count of pixels for all types of land cover within a given radius buffer. MODIS Level 3 monthly average NDVI products with a spatial resolution of 0.1° ($\approx$10 km) during the study period were downloaded from the NASA Earth Observatory (http://neo.sci.gsfc.nasa.gov/). Further information about these data products has been previously described (Hamm et al., 2015b).

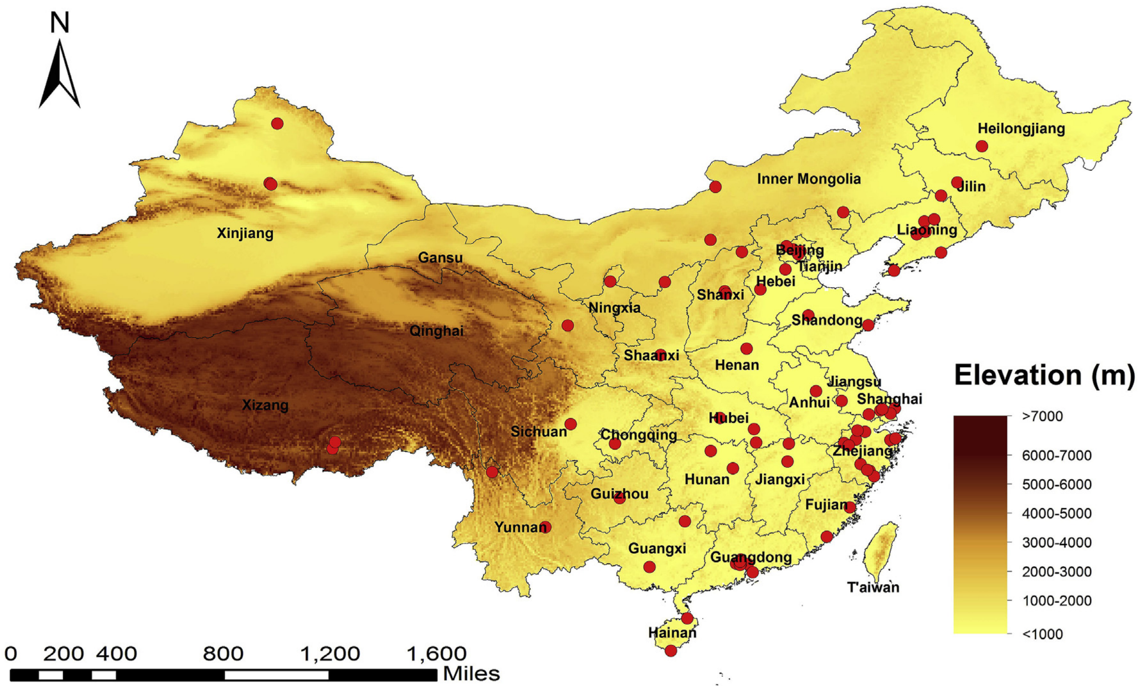

Fig. 1. Locations of 77 stations with ground-based measurements of PM_1 and $PM_{2.5}$.

2.5. Other spatial predictors

Aqua and Terra active fires during the study period were downloaded from NASA Fire Information for Resource Management System (https://earthdata.nasa.gov/data/near-real-time-data/firms) (Hu et al., 2014a). Daily counts of fire spots within a buffer of 75 km were calculated for each ground monitoring station and grid cell created. The global Shuttle Radar Topography Mission (SRTM) Digital Elevation Model (DEM) has a resolution of 3 arc-seconds (approximately 90 m) (Hamm et al., 2015b). SRTM version 4 elevation data for China were downloaded from The CGIAR Consortium for Spatial Information (http://srtm.csi.cgiar.org/). The elevation for each monitoring station was extracted and mean value of all elevation pixels fell in each grid cell was calculated.

2.6. Model development and validation

A 0.1-degree grid ($\approx$10 km) covering China with 96 104 grid cells was created to integrate spatial and temporal predictors and develop models. Daily values of meteorological variables were interpolated for each grid cell based on daily meteorological data from 824 weather stations. For predictors with a resolution of 0.1° (e.g., AOD, meteorological variables and NDVI), values were directly extracted for each grid cells. For predictors with a resolution higher than 0.1° (e.g., land cover and elevation), mean values of all pixels of predictors in each grid cell were calculated and used for prediction. Monthly and annual predictors (e.g., NDVI, urban cover and forest cover) were linked with daily predictors according to the month or year they were collected, as the values of those variables are unlikely to change within one month or year, respectively. All spatial and temporal predictors were integrated into the grid for each grid cell by location (longitude and latitude of the centroid) and calendar date. In this study, the ground monitoring data of PM_1 was only available for 9 months from November 2013 to July 2014, and $PM_{2.5}$ data covered 15 months from September 2013 to December 2014. Based on the high correlation between PM_1 and $PM_{2.5}$ concentrations and their relationships with temperature and relative humidity (Lee et al., 2006b; Li et al., 2015; Wang et al., 2015), daily concentrations of PM_1 at the 77 stations during the periods from Sep 2013 to Nov 2013 and from Jul 2014 to Dec 2014 were interpolated with the following generalised additive model (GAM):

$$PM_1 = s(PM_{2.5}) + s(TEMP) + s(RH)$$

where: *TEMP* and *RH* refer to daily mean temperature and relative humidity, respectively. The degrees of freedom for smooth terms were automatically selected by GAM. This interpolation was performed for each of 77 stations separately and together it captured a large proportion of variability in PM_1 ($R^2 = 93\%$). The interpolated PM_1 data covering 15 months were more suitable than the original 9-month ground monitoring data to capture temporal trends and seasonality of PM_1 concentrations.

AOD, meteorological variables, and elevation were determined at each measurement point, while land use variables were determined at a range of buffers from 100 m to 10 km (Knibbs et al., 2014). The total number of active fires within 75 km of each site was counted (Hu et al., 2014c).

Our approach to model development was informed by recent $PM_{2.5}$ studies in China that described predictor variables were also potentially associated with PM_1 (Fang et al., 2016; Ma et al., 2014, 2015). We used a GAM and began by including AOD and then incrementally included other predictors until we reached a parsimonious model that explained the most variability in PM_1. For land use variables calculated at different buffers that were associated with PM_1, we included the buffer distance that offered greatest ability to explain PM_1. We arrived at the following GAM as being the best model for predicting daily concentrations of PM_1:

$$PM_1 = AOD_c \times province + s(TEMP) \times province + s(RH) \times province + s(WS) \times province + s(BP) + firesmoke \times province + NDVI \times province + Forest\_cover + Urban\_cover$$

+ Water_areas + month + Dayofweek + log(elev)

where: AOD_c is the combined AOD; *province* is the province where the station was located and it is an interaction term to account for the regional variations of PM_1-AOD association; *TEMP* is daily mean temperature (°C); *RH* is daily mean relative humidity (%); *WS* is daily mean wind speed (km/h); *BP* is daily mean barometric pressure (kPa); *firesmoke* is the count of fire smoke spots; *NDVI* is the monthly average NDVI value; *Forest_cover* is the percentage of forest cover (3-km radius buffer); *Urban_cover* is the percentage of urban cover (10-km radius buffer); *Water_areas* is the percentage of water areas (10-km radius buffer); log*(elev)* is the log transformed elevation (m). The degrees of freedom for smoothed terms were automatically selected by GAM.

Although our dependent variable was daily PM_1 in the period from September 2013 to December 2014, we also wanted to demonstrate the feasibility of longer-term (i.e., decadal) estimation of PM_1. We thus used our final GAM to predict daily concentrations of PM_1 for each grid cell created from 2005 to 2014 by capitalizing on historical predictor data, including AOD and meteorological observations. We also averaged our daily predictions to obtain monthly and seasonal estimates of PM_1.

To assess the validity of our predictions, a 10-fold cross-validation (CV) process was performed using data from 48 days (of the 478 days total) randomly selected as test set and the rest of the data as the training set. This process was repeated 500 times. The overall adjusted R^2 and Root Mean Square Error (RMSE) were calculated. Sensitivity analyses were also performed to test the model's robustness. For example, we added daily hours of sunshine and population density in the final model to check whether they improved model performance. We also included other temporal predictions (e.g., day of year, season) in the model replacing calendar month.

3. Results

In total, 32,675 records of ground-monitored PM_1 data from September 2013 through December 2014 were included in the model development. The mean concentration of ground-measured PM_1 was 39.1 μg/m^3. The lowest level of PM_1 was observed in Shangri-La (5.0 μg/m^3), Yunnan Province, while the highest was in Shijiazhuang (82.1 μg/m^3), Heibei Province. Summaries of ground-based measurements of PM_1 and weather conditions at the 77 PM_1 monitoring stations are shown in Tables S2–S6 in the Supplemental Material.

Table 1 shows the improvement in performance of the best daily GAM with the addition of each successive predictor. The daily AOD-only model for PM_1 showed an R^2 of 24%. In other models, meteorological variables, especially temperature and relative humidity, made the greatest contribution to the model performance. The model with AOD, and meteorological predictors (temperature and relative humidity) had an R^2 of 40%. Fig. 2 shows the performance of final model for predicting PM_1 concentrations (step 13 in Table 1), which explained 58% of the variability in daily PM_1 (RMSE = 21.7 μg/m^3). The 10-fold cross-validation showed modest prediction errors with little bias (Fig. 3). The CV R^2 for daily estimation was 59% (RMSE = 22.5 μg/m^3, slope = 1.01).

Daily concentrations of PM_1 were estimated and the results were averaged to monthly and seasonal mean concentrations. Monthly and seasonal estimations were improved (R^2 = 0.74 and 0.82, respectively, RMSE = 12.0 μg/m^3 and 9.0 μg/m^3, respectively) (Fig. 2). The 10-fold cross-validation shows that higher predictive ability was observed for monthly estimation (R^2 = 71%, RMSE = 13.0 μg/m^3, slope = 0.96) and seasonal estimation (R^2 = 77%, RMSE = 11.4 μg/m^3, slope = 1.02) (Fig. 3).

Sensitivity analyses showed that our results were robust; adding hours of sunshine and population density did not improve the model performance, and calendar month is more suitable than day of year or season to account for the long-term trend in PM_1. Results of the sensitivity analyses are shown in Table S8 in the Supplemental Material.

Fig. 4 shows the estimated mean concentrations of PM_1 during 2005 through 2014. The mean concentration of PM_1 predicted across China was 26.9 μg/m^3. The highest levels of PM_1 (≥70 μg/m^3) were predicted in South-Western Hebei, Beijing and Tianjin. Relatively high levels of PM_1 (≥50 μg/m^3 and <70 μg/m^3) were present in Sichuan, Chongqing, Henan and Liaoning. The lowest levels of PM_1 (<20 μg/m^3) were shown in South-Western and Northern remote areas of China including Xizang, Yunnan and Northern Inner Mongolia.

Fig. 5 shows the estimated seasonal concentrations of PM_1 across China with the highest levels predicted in winter (mean = 45.3 μg/m^3) and the lowest in summer (mean = 15.7 μg/m^3). The levels of PM_1 we estimated were similar in spring and in autumn (26.4 μg/m^3 and 25.9 μg/m^3, respectively). Areas in North-Eastern China and South-Western Hebei exhibited a substantial increase from summer to winter.

Fig. 6 shows the 10-year trends (2005–2014) in PM_1 concentrations estimated in both heavily polluted regions and across the entire country. The estimated PM_1 levels in China as a whole exhibited slight increases, with an increase of 2.1 μg/m^3 from 2005 to 2014. Modest changes of PM_1 levels were observed in Guangdong, Yangtze River Delta and North-Eastern China. Increased trends of PM_1 during the past decade were present in South-Western Hebei (increased by 8.9 μg/m^3), Beijing and Tianjin (increased by 8.6 μg/m^3) and Chongqing and Eastern Sichuan (increased by 6.5 μg/m^3). Locations of these heavy polluted regions are shown in Fig. S3 in the Supplementary Material.

4. Discussion

Despite China's well-publicized air pollution problems, studies on the long-term effects of fine particulate matter on health are limited due to the lack of ground-level monitoring data, especially prior to 2013. Statistical models using satellite-retrieved AOD have the potential to estimate historical and current exposures to particulate matter with good accuracy and spatial resolution by exploiting the relatively strong relationship between $PM_{2.5}$ and AOD over China, as demonstrated by previous studies (Lee et al., 2011; Wang and Christopher, 2003; Zhang et al., 2009). To the best of our knowledge, this is the first study to estimate PM_1 in China using satellite remote sensing. Using a combination of MODIS AOD data and other spatiotemporal predictors, we estimated daily, monthly and seasonal levels of PM_1 from 2005 through 2014 at a resolution of 0.1° across China. We captured 59%, 71%, and 77% of variability in daily, seasonal and monthly PM1 during 2013–14, which we then applied to estimate historical levels during the preceding decade.

Although only 77 ground monitoring sites were included in this study because PM_1 is not routinely monitored, the results of cross-validation indicated the predictive ability of our model is comparable to that reported in previous study of $PM_{2.5}$ in China based on much larger set of ground monitoring data (Ma et al., 2015). Studies have demonstrated satellite-retrieved AOD is strongly linked with particles between 0.1 and 2.0 μm (Diner et al., 1998; Kahn et al., 2001), and the particle size of PM_1 is right within that range. Additionally, ground monitoring data indicated ambient PM_1 accounted for 66%–91% of $PM_{2.5}$ in China, and with PM_1 and meteorological factors, most variations of $PM_{2.5}$ concentrations can be explained (Lee et al., 2006a; Wang et al., 2015).

Table 1
Steps for selecting the best model for predicting daily PM_1.

Step	Variable in model	R^2 (adj)	GCV
1	AOD*	25%	914.3
2	AOD*+Temperature*	36%	778.8
3	AOD*+Temperature*+Relative humidity*	40%	731.2
4	AOD*+Temperature*+Relative humidity*+Wind speed*	43%	697.0
5	AOD*+Temperature*+Relative humidity*+Wind speed*+Barometric pressure	43%	696.9
6	AOD*+Temperature*+Relative humidity*+Wind speed*+Barometric pressure + Month	49%	628.8
7	AOD*+Temperature*+Relative humidity*+Wind speed*+Barometric pressure + Month + Forest Cover	49%	623.6
8	AOD*+Temperature*+Relative humidity*+Wind speed*+Barometric pressure + Month + Forest Cover + Urban Cover	49%	622.4
9	AOD*+Temperature*+Relative humidity*+Wind speed*+Barometric pressure + Month + Forest Cover + Urban Cover + Water Cover	49%	622.3
10	AOD*+Temperature*+Relative humidity*+Wind speed*+Barometric pressure + Month + Forest Cover + Urban Cover + Water Cover + Fire smoke*	50%	619.2
11	AOD*+Temperature*+Relative humidity*+Wind speed*+Barometric pressure + Month + Forest Cover + Urban Cover + Water Cover + Fire smoke*+NDVI*	52%	587.4
12	AOD*+Temperature*+Relative humidity*+Wind speed*+Barometric pressure + Month + Forest Cover + Urban Cover + Water Cover + Fire smoke*+NDVI*+Day of week	53%	585.0
13	AOD*+Temperature*+Relative humidity*+Wind speed*+Barometric pressure + Month + Forest Cover + Urban Cover + Water Cover + Fire smoke*+NDVI*+Day of week + Elevation	58%	522.5

*Refers to variables with "province" as an interaction term in the model.

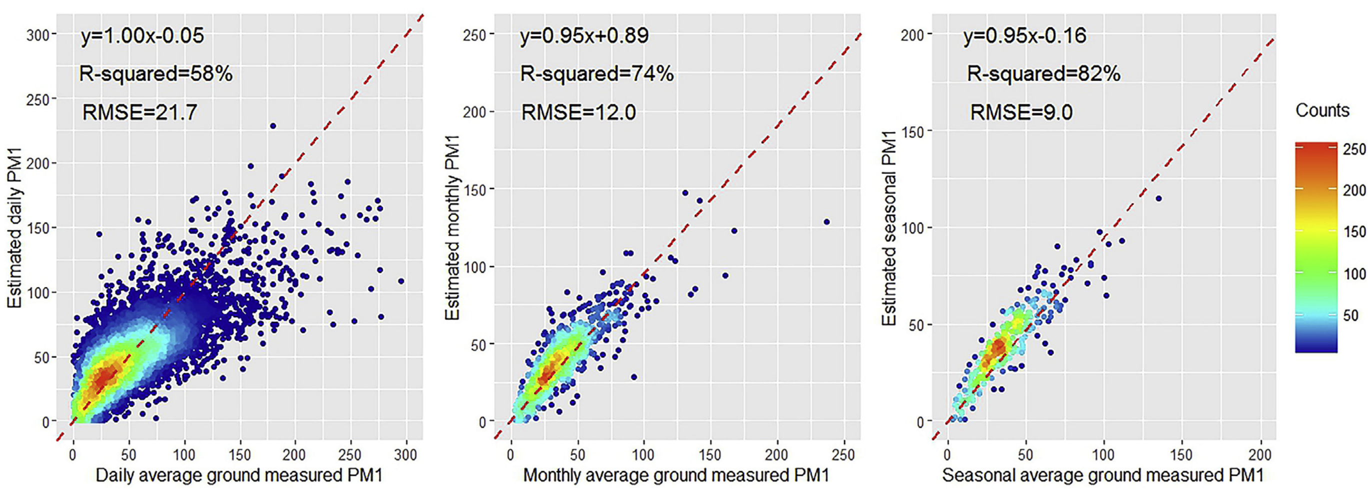

Fig. 2. Scatterplots of model fitting for daily, monthly and seasonal estimation of PM_1 concentrations ($\mu g/m^3$).

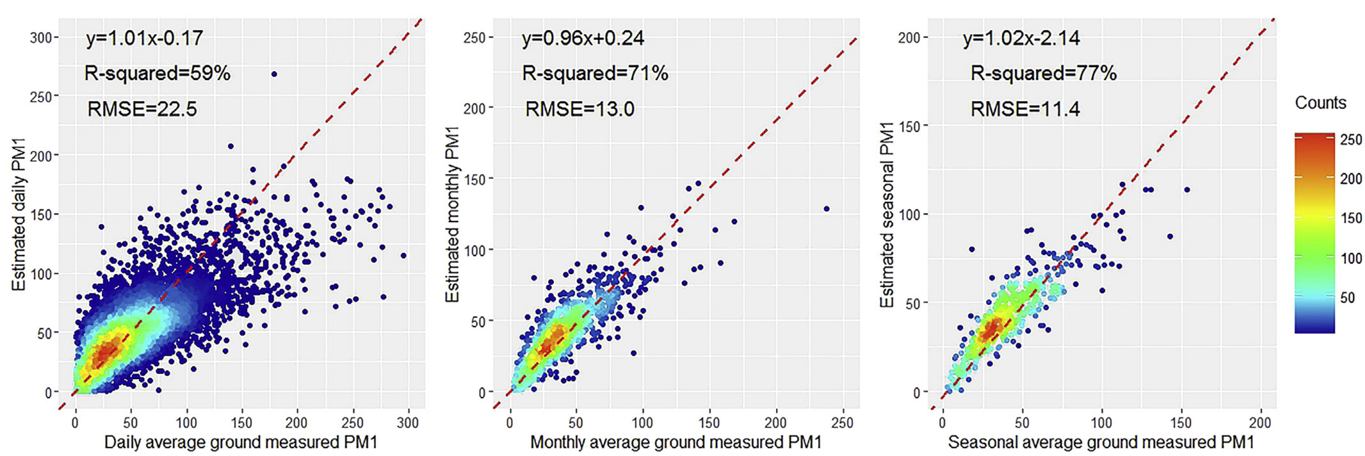

Fig. 3. Scatterplots of 10-fold cross-validation for daily, monthly and seasonal estimation of PM_1 concentrations ($\mu g/m^3$).

The overall temporal trends and seasonality of PM_1 in China in our study were also consistent with previous studies on $PM_{2.5}$, although we observed with minor differences in the locations of more and less polluted areas. For example, estimated levels of PM_1 in some heavily-polluted regions were relatively high but not the highest observed in our study including the Yangtze River Delta Region and Pearl River Delta Region. These are the locations where the highest levels of $PM_{2.5}$ were estimated in previous studies (Ma

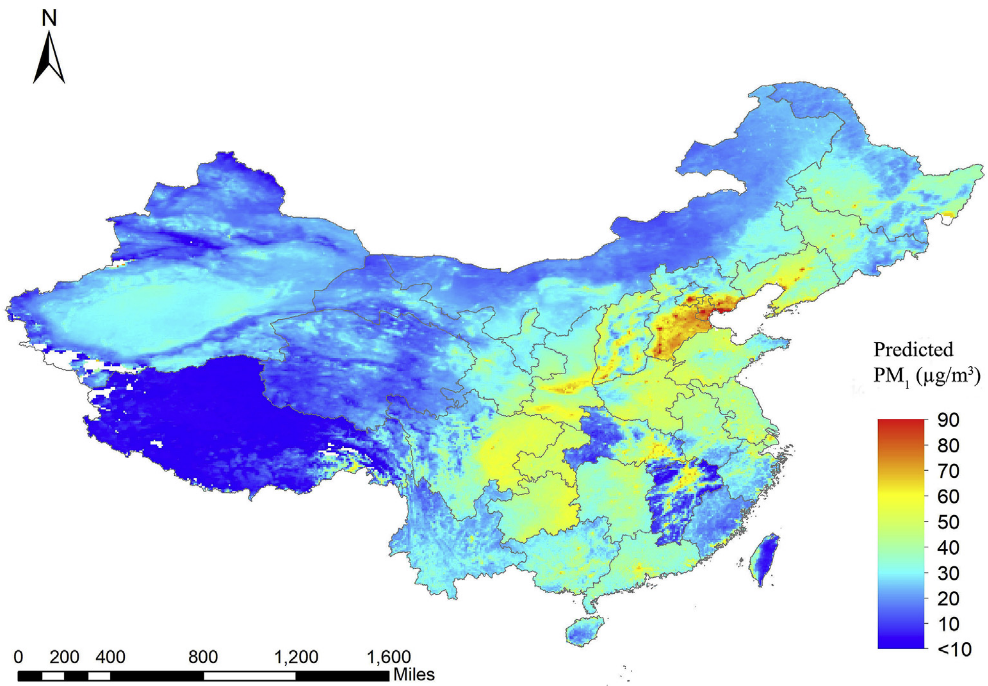

Fig. 4. Annual mean concentrations of PM_1 (μg/m^3) in China from 2005 to 2014.

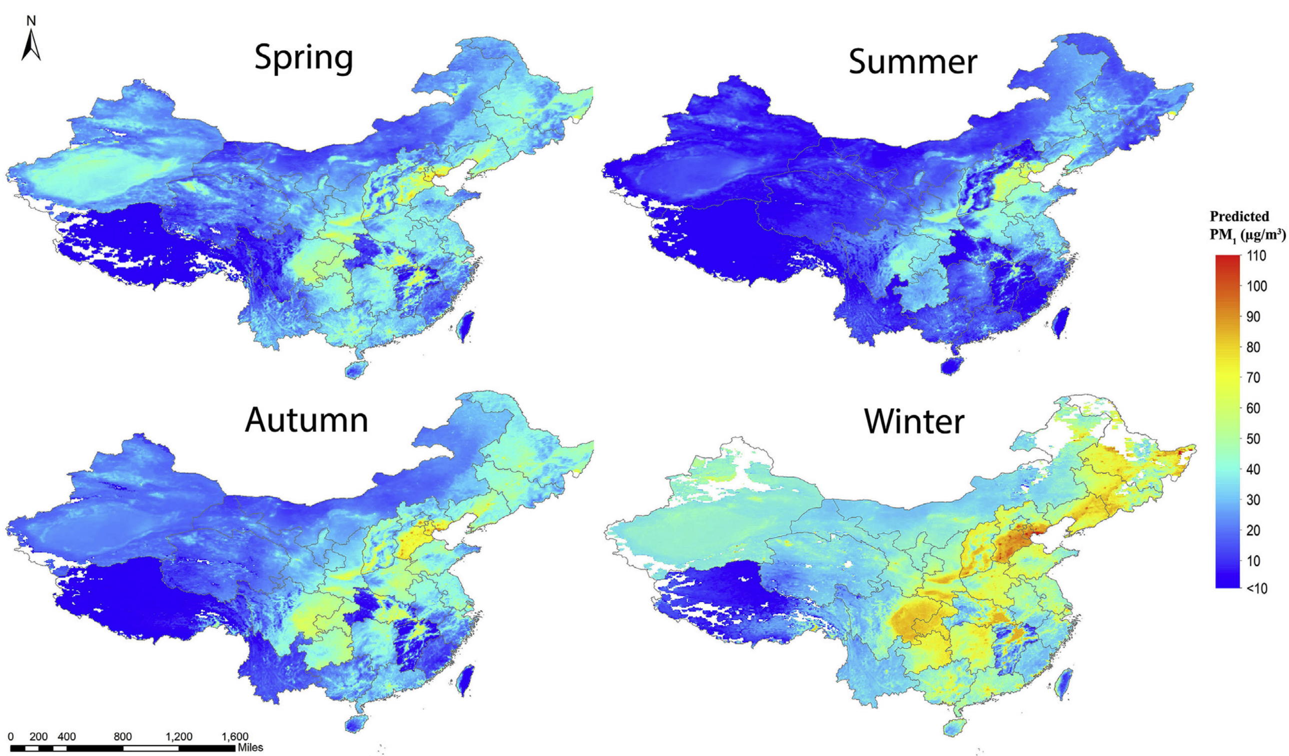

Fig. 5. Mean concentrations of PM_1 (μg/m^3) in four seasons in China from 2005 to 2014.

et al., 2015; Zheng et al., 2016). This difference could be due to the fact the major sources of PM_1 and $PM_{2.5}$ do not necessarily contribute to the same extent for both size fractions (Cabada et al., 2004; Vecchi et al., 2004). For example, combustion process including biomass burning can make a relatively greater contribution to ambient PM_1 than $PM_{2.5}$ (Perrone et al., 2013), and the contributions can be seasonally-dependent (Lee et al., 2006a).

Although, to our knowledge, no national studies on estimating PM_1 in other countries have been reported, the predicted PM_1 level of China in this study was much higher than those reported by some regional studies in western countries (Pérez et al., 2008, 2010; Viana et al., 2003). The often severe particulate matter air pollution

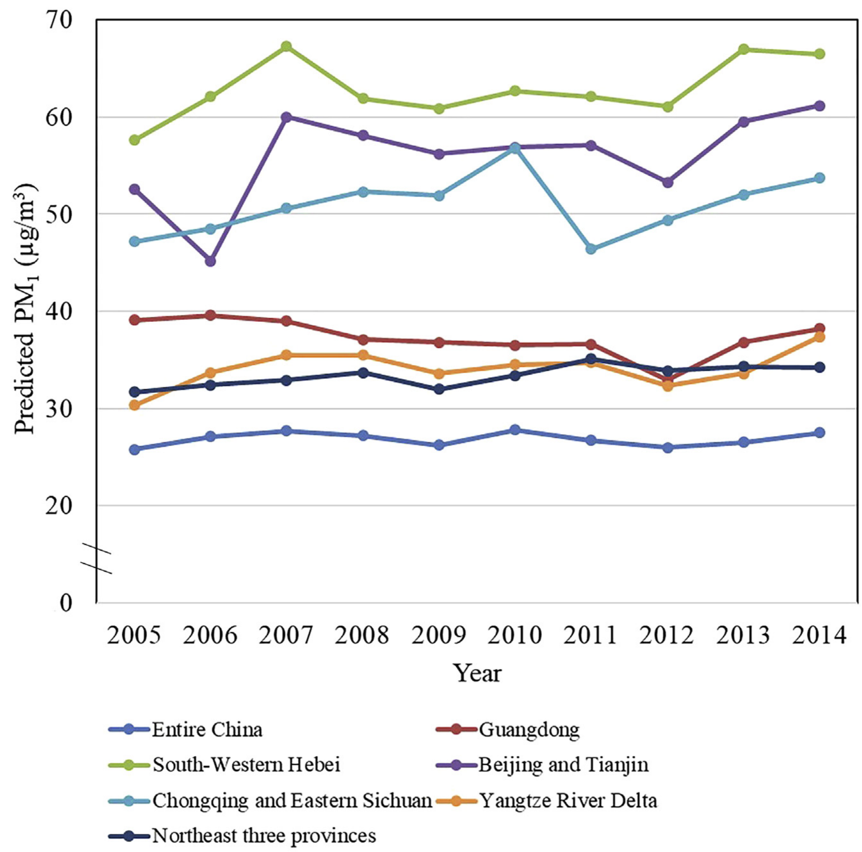

Fig. 6. Trends of PM_1 concentrations ($\mu g/m^3$) in heavily polluted regions and the entire China from 2005 to 2014.

in China is mainly caused by coal combustion, traffic and industrial emissions which are associated with the rapid economic development and expansion of the urban population, especially for mega cities including Beijing, Shanghai, Guangzhou and Shenzhen (Chan and Yao, 2008; Xu et al., 2013). In this study, the highest estimated levels of PM_1 occurred in the South-Western Hebei, Chongqing and Sichuan. The heavy air pollution in South-Western Hebei could be originated from dense local population and industries of steel and power (Wang et al., 2014). The high levels of PM_1 estimated in Sichuan and Chongqing might be due to the local landscape. The basin-like topography is also characterized by low wind speed which slow down the dilution of airborne pollutants due to frequent temperature inversions (Li et al., 2015). In addition, rapid industrial and economic growth are apparent in the Sichuan Basin. High levels of PM_1 were also present in North-Eastern China during winter season, which might be linked with the cold climate where local coal-based heating is used for more than 6 months each year (Ma et al., 2010). Furthermore, this area is highly industrialized part of China which contributes to poor air quality (Sun et al., 2010).

The satellite-retrieved AOD was used to demonstrate the potential to predict recent and historical levels of PM_1. Other studies have reported the predicted $PM_{2.5}$ levels across China using MODIS AOD data with CV R^2 values ranging from 73% to 82% (Fang et al., 2016; Ma et al., 2015; You et al., 2016; Zhang et al., 2016). Although the predictive ability of our PM_1 models did not exceed those studies, it could plausibly be improved by greater numbers of PM_1 monitors, similar to the $PM_{2.5}$ monitoring network (Hamm et al., 2016). Apart from ground-level measurements of air pollutants, the predictive ability could be improved by adding traffic and road information in the model, considering traffic emissions are main sources of outdoor air pollution (Hamra et al., 2015; Künzli et al., 2000). Further improvements may also be found by including the outputs from chemical transport models (CTMs) in statistical models. The benefit of this has been demonstrated for PM_{10}, $PM_{2.5}$ and NO_2 (de Hoogh et al., 2016; Hamm et al., 2015a).

With the use of satellite-retrieved AOD data, this study estimated the temporal and spatial variations of ambient PM_1 concentrations across China during past decade. We hope it will provide information for policy makers to allocate resources for the prevention and control of severe particulate matter air pollution in China, especially for some heavy-polluted regions. Moreover, the results of this study have the potential to link with a range of health data to further explore the adverse health effects of PM_1.

However, this study has some limitations. We had limited ground monitoring data from 77 stations included in this study and sparse data for Western China especially, including Xinjiang, Xizang, Qinghai and Gansu Province. The prediction of PM_1 during 2005–14 in this study is based on an assumption that the relationship between PM_1 and its predictor variables remained consistent over this time. However, this assumption cannot be verified in China due to unavailability of ground monitoring data prior to 2013. Also, although DT and DB AOD data were downloaded separately and combined to fill in the missing values, a high proportion of missing AOD values still existed which limits the ability to detect the daily patterns of PM_1 concentrations in China. Finally, to improve predictive ability, we included province as a fixed-effect term in the models for prediction. The disadvantage of this approach is that it produces discontinuity at boundaries in some provinces. PM_1, with its smaller particle size than $PM_{2.5}$, might be more harmful on human health than $PM_{2.5}$ (Lin et al., 2016). Considering the importance of PM_1 and its potential strong associations with health in China, more exposure data should be obtained and future studies should further explore its spatial and temporal distributions.

5. Conclusion

Statistical models using satellite-retrieved AOD, land use information and meteorology could capture the spatial and temporal variability in ground-level PM_1 concentrations in China. This is the first study to estimate historical levels of PM_1 with satellite remote sensing. It provides important quantitative information regarding the distribution of PM_1 across China. The results have the potential to link with a wide range of health data and help understand health outcomes in a high pollution country. Given greater ground-based measurements of PM_1 as well as environmental data and the output of chemical transport models (CTMs), the predictive ability of our models could be extended and improved.

Competing financial interests

The authors declare they have no actual or potential competing financial interests.

Acknowledgements

Y.G. was supported by Career Development Fellowship of Australian National Health and Medical Research Council (NHMRC, APP1107107). S.L. was supported by the NHMRC Early Career Fellowship (APP1109193) and Seed Funding from the NHMRC Centre of Research Excellence (CRE)–Centre for Air quality and health Research and evaluation (APP1030259). G.C. was supported by China Scholarship Council (CSC).

Appendix A. Supplementary data

Supplementary data related to this article can be found at https://doi.org/10.1016/j.envpol.2017.10.011.

References

Cabada, J.C., Pandis, S.N., Subramanian, R., Robinson, A.L., Polidori, A., Turpin, B., 2004. Estimating the secondary organic aerosol contribution to PM2.5Using the EC tracer method special issue of aerosol science and technologyon findings from the fine particulate matter supersites program. Aerosol Sci. Technol. 38, 140–155.
Cao, J., Xu, H., Xu, Q., Chen, B., Kan, H., 2012. Fine particulate matter constituents and cardiopulmonary mortality in a heavily polluted Chinese city. Environ. Health Perspect. 120, 373.
Chan, C.K., Yao, X., 2008. Air pollution in mega cities in China. Atmos. Environ. 42, 1–42.
Chen, G., Li, S., Zhang, Y., Zhang, W., Li, D., Wei, X., He, Y., Bell, M.L., Williams, G., Marks, G.B., 2017. Effects of ambient PM 1 air pollution on daily emergency hospital visits in China: an epidemiological study. Lancet Planet. Health 1, e221–e229.
de Hoogh, K., Gulliver, J., van Donkelaar, A., Martin, R.V., Marshall, J.D., Bechle, M.J., Cesaroni, G., Pradas, M.C., Dedele, A., Eeftens, M., 2016. Development of West-European PM 2.5 and NO 2 land use regression models incorporating satellite-derived and chemical transport modelling data. Environ. Res. 151, 1–10.
Diner, D.J., Beckert, J.C., Reilly, T.H., Bruegge, C.J., Conel, J.E., Kahn, R.A., Martonchik, J.V., Ackerman, T.P., Davies, R., Gerstl, S.A., 1998. Multi-angle Imaging SpectroRadiometer (MISR) instrument description and experiment overview. Ieee Trans. Geosci. Remote Sens. 36, 1072–1087.
Dockery, D.W., Stone, P.H., 2007. Cardiovascular risks from fine particulate air pollution. N. Engl. J. Med. 356, 511–513.
Fang, X., Zou, B., Liu, X., Sternberg, T., Zhai, L., 2016. Satellite-based ground PM 2.5 estimation using timely structure adaptive modeling. Remote Sens. Environ. 186, 152–163.
Friedl, M.A., Sulla-Menashe, D., Tan, B., Schneider, A., Ramankutty, N., Sibley, A., Huang, X., 2010. MODIS Collection 5 global land cover: algorithm refinements and characterization of new datasets. Remote Sens. Environ. 114, 168–182.
Furrer, R., Nychka, D., Sain, S., Nychka, M.D., 2009. Package 'fields'. R Foundation for Statistical Computing. Vienna, Austria. http://www.idg.pl/mirrors/CRAN/web/packages/fields/fields.pdf. last accessed 22 December 2012.
Grimm, H., Eatough, D.J., 2009. Aerosol measurement: the use of optical light scattering for the determination of particulate size distribution, and particulate mass, including the semi-volatile fraction. J. Air & Waste Manag. Assoc. 59, 101–107.
Guo, J., Xia, F., Zhang, Y., Liu, H., Li, J., Lou, M., He, J., Yan, Y., Wang, F., Min, M., 2017. Impact of diurnal variability and meteorological factors on the PM 2.5-AOD relationship: implications for PM 2.5 remote sensing. Environ. Pollut. 221, 94–104.
Guo, J., Zhang, X., Che, H., Gong, S., An, X., Cao, C.-X., Guang, J., Zhang, H., Wang, Y.-Q., Zhang, X.-C., 2009. Correlation between PM concentrations and aerosol optical depth in eastern China. Atmos. Environ. 43, 5876–5886.
Hamm, N.A.S., Finley, A.O., Schaap, M., Stein, A., 2015a. A spatially varying coefficient model for mapping PM10 air quality at the European scale. Atmos. Environ. 102, 393–405.
Hamm, N.A.S., Soares Magalhaes, R.J., Clements, A.C., 2015b. Earth observation, spatial data quality, and neglected tropical diseases. PLoS Negl. Trop. Dis. 9, e0004164.
Hamm, N.A.S., van Lochem, M., Hoek, G., Otjes, R., van der Sterren, S., Verhoeven, H., 2016. In: Close, J.-P. (Ed.), "The Invisible Made Visible": Science and Technology. AiREAS: Sustainocracy for a Healthy City. Springer, pp. 51–77.
Hamra, G.B., Laden, F., Cohen, A.J., Raaschou-Nielsen, O., Brauer, M., Loomis, D., 2015. Lung cancer and exposure to nitrogen dioxide and traffic: a systematic review and meta-analysis. Environ. Health Perspect. 123, 1107–1112.
Hu, Waller, L.A., Lyapustin, A., Wang, Y., Liu, Y., 2014a. Improving satellite-driven PM less than 2.5 micrometer models with moderate resolution imaging spectroradiometer fire counts in the southeastern US.
Hu, X., Waller, L.A., Lyapustin, A., Wang, Y., Liu, Y., 2014b. 10-year spatial and temporal trends of PM2.5 concentrations in the southeastern US estimated using high-resolution satellite data. Atmos. Chem. Phys. 14, 6301–6314.
Hu, X., Waller, L.A., Lyapustin, A., Wang, Y., Liu, Y., 2014c. Improving satellite-driven PM2. 5 models with Moderate Resolution Imaging Spectroradiometer fire counts in the southeastern US. J. Geophys. Res. Atmos. 119.
Jing-Mei, Y., Jin-Huan, Q., Yan-Liang, Z., 2010. Validation of aerosol optical depth from Terra and Aqua MODIS retrievals over a tropical coastal site in China. Atmos. Ocean. Sci. Lett. 3, 36–39.
Just, A.C., Wright, R.O., Schwartz, J., Coull, B.A., Baccarelli, A.A., Tellez-Rojo, M.M., Moody, E., Wang, Y., Lyapustin, A., Kloog, I., 2015. Using high-resolution satellite aerosol optical depth to estimate daily PM2.5 geographical distribution in Mexico city. Environ. Sci. Technol. 49, 8576–8584.
Kahn, R., Banerjee, P., McDonald, D., 2001. Sensitivity of multiangle imaging to natural mixtures of aerosols over ocean. J. Geophys. Res. Atmos. 106, 18219–18238.
Kan, H., Chen, B., Hong, C., 2009. Health impact of outdoor air pollution in China: current knowledge and future research needs. Environ. Health Perspect. 117, A187.
Kloog, I., Nordio, F., Coull, B.A., Schwartz, J., 2012. Incorporating local land use regression and satellite aerosol optical depth in a hybrid model of spatiotemporal PM2.5 exposures in the Mid-Atlantic states. Environ. Sci. Technol. 46, 11913–11921.
Knibbs, L.D., Hewson, M.G., Bechle, M.J., Marshall, J.D., Barnett, A.G., 2014. A national satellite-based land-use regression model for air pollution exposure assessment in Australia. Environ. Res. 135, 204–211.
Koelemeijer, R., Homan, C., Matthijsen, J., 2006. Comparison of spatial and temporal variations of aerosol optical thickness and particulate matter over Europe. Atmos. Environ. 40, 5304–5315.
Künzli, N., Kaiser, R., Medina, S., Studnicka, M., Chanel, O., Filliger, P., Herry, M., Horak, F., Puybonnieux-Texier, V., Quénel, P., Schneider, J., Seethaler, R., Vergnaud, J.C., Sommer, H., 2000. Public-health impact of outdoor and traffic-related air pollution: a European assessment. Lancet 356, 795–801.
Lee, H., Liu, Y., Coull, B., Schwartz, J., Koutrakis, P., 2011. A novel calibration approach of MODIS AOD data to predict PM2. 5 concentrations. Atmos. Chem. Phys. 11, 7991–8002.
Lee, S., Cheng, Y., Ho, K., Cao, J., Louie, P.-K., Chow, J., Watson, J., 2006a. PM1. 0 and PM2. 5 characteristics in the roadside environment of Hong Kong. Aerosol Sci. Technol. 40, 157–165.
Lee, S.C., Cheng, Y., Ho, K.F., Cao, J.J., Louie, P.K.K., Chow, J.C., Watson, J.G., 2006b. PM1.0 and PM2.5 characteristics in the roadside environment of Hong Kong. Aerosol Sci. Technol. 40, 157–165.
Levy, R., Mattoo, S., Munchak, L., Remer, L., Sayer, A., Patadia, F., Hsu, N., 2013. The Collection 6 MODIS aerosol products over land and ocean. Atmos. Meas. Tech. 6, 2989–3034.
Li, Y., Chen, Q.L., Zhao, H.J., Wang, L., Tao, R., 2015. Variations in PM10, PM2.5 and PM1.0 in an urban area of the sichuan basin and their relation to meteorological factors. Atmosphere 6, 150–163.
Lin, H., Tao, J., Du, Y., Liu, T., Qian, Z., Tian, L., Di, Q., Rutherford, S., Guo, L., Zeng, W., 2016. Particle size and chemical constituents of ambient particulate pollution associated with cardiovascular mortality in Guangzhou, China. Environ. Pollut. 208, 758–766.
Ma, W.-L., Li, Y.-F., Qi, H., Sun, D.-Z., Liu, L.-Y., Wang, D.-G., 2010. Seasonal variations of sources of polycyclic aromatic hydrocarbons (PAHs) to a northeastern urban city, China. Chemosphere 79, 441–447.
Ma, Y., Chen, R., Pan, G., Xu, X., Song, W., Chen, B., Kan, H., 2011. Fine particulate air pollution and daily mortality in Shenyang, China. Sci. Total Environ. 409, 2473–2477.
Ma, Z., Hu, X., Sayer, A.M., Levy, R., Zhang, Q., Xue, Y., Tong, S., Bi, J., Huang, L., Liu, Y., 2015. Satellite-based spatiotemporal trends in PM concentrations: China, 2004-

2013. Environ. Health Perspect. 124, 184–192.
Ma, Z.W., Hu, X.F., Huang, L., Bi, J., Liu, Y., 2014. Estimating ground-level PM2.5 in China using satellite remote sensing. Environ. Sci. Technol. 48, 7436–7444.
Meng, X., Fu, Q., Ma, Z., Chen, L., Zou, B., Zhang, Y., Xue, W., Wang, J., Wang, D., Kan, H., Liu, Y., 2015. Estimating ground-level PM in a Chinese city by combining satellite data, meteorological information and a land use regression model. Environ. Pollut. 208, 177–184.
Pérez, N., Pey, J., Cusack, M., Reche, C., Querol, X., Alastuey, A., Viana, M., 2010. Variability of particle number, black carbon, and PM10, PM2. 5, and PM1 levels and speciation: influence of road traffic emissions on urban air quality. Aerosol Sci. Technol. 44, 487–499.
Pérez, N., Pey, J., Querol, X., Alastuey, A., López, J., Viana, M., 2008. Partitioning of major and trace components in PM 10–PM 2.5–PM 1 at an urban site in Southern Europe. Atmos. Environ. 42, 1677–1691.
Perrone, M., Becagli, S., Orza, J.G., Vecchi, R., Dinoi, A., Udisti, R., Cabello, M., 2013. The impact of long-range-transport on PM1 and PM2. 5 at a Central Mediterranean site. Atmos. Environ. 71, 176–186.
Rohde, R.A., Muller, R.A., 2015. Air pollution in China: mapping of concentrations and sources. PLoS One 10, e0135749.
Sayer, A., Hsu, N., Bettenhausen, C., Jeong, M.J., 2013. Validation and uncertainty estimates for MODIS Collection 6 “Deep Blue” aerosol data. J. Geophys. Res. Atmos. 118, 7864–7872.
Sun, Y., Zhou, Q., Xie, X., Liu, R., 2010. Spatial, sources and risk assessment of heavy metal contamination of urban soils in typical regions of Shenyang, China. J. Hazard Mater 174, 455–462.
Vecchi, R., Marcazzan, G., Valli, G., Ceriani, M., Antoniazzi, C., 2004. The role of atmospheric dispersion in the seasonal variation of PM1 and PM2. 5 concentration and composition in the urban area of Milan (Italy). Atmos. Environ. 38, 4437–4446.
Viana, M., Querol, X., Alastuey, A., Gangoiti, G., Menéndez, M., 2003. PM levels in the Basque Country (Northern Spain): analysis of a 5-year data record and interpretation of seasonal variations. Atmos. Environ. 37, 2879–2891.
Wang, J., Christopher, S.A., 2003. Intercomparison between satellite-derived aerosol optical thickness and PM2. 5 mass: implications for air quality studies. Geophys. Res. Lett. 30.
Wang, L., Wei, Z., Yang, J., Zhang, Y., Zhang, F., Su, J., Meng, C., Zhang, Q., 2014. The 2013 severe haze over southern Hebei, China: model evaluation, source apportionment, and policy implications. Atmos. Chem. Phys. 14, 3151–3173.
Wang, Y.Q., Zhang, X.Y., Sun, J.Y., Zhang, X.C., Che, H.Z., Li, Y., 2015. Spatial and temporal variations of the concentrations of PM10, PM2.5 and PM1 in China. Atmos. Chem. Phys. 15, 13585–13598.
Xu, P., Chen, Y., Ye, X., 2013. Haze, air pollution, and health in China. Lancet 382, 2067.
Yang, C., Peng, X., Huang, W., Chen, R., Xu, Z., Chen, B., Kan, H., 2012. A time-stratified case-crossover study of fine particulate matter air pollution and mortality in Guangzhou, China. Int. Arch. Occup. Environ. Health 85, 579–585.
You, W., Zang, Z., Zhang, L., Li, Y., Wang, W., 2016. Estimating national-scale ground-level PM25 concentration in China using geographically weighted regression based on MODIS and MISR AOD. Environ. Sci. Pollut. Res. 23, 8327–8338.
Zhang, H., Hoff, R.M., Engel-Cox, J.A., 2009. The relation between Moderate Resolution Imaging Spectroradiometer (MODIS) aerosol optical depth and PM2. 5 over the United States: a geographical comparison by US Environmental Protection Agency regions. J. Air & Waste Manag. Assoc. 59, 1358–1369.
Zhang, T., Liu, G., Zhu, Z., Gong, W., Ji, Y., Huang, Y., 2016. Real-time estimation of satellite-derived PM2. 5 based on a semi-physical geographically weighted regression model. Int. J. Environ. Res. Public Health 13, 974.
Zheng, Y., Zhang, Q., Liu, Y., Geng, G., He, K., 2016. Estimating ground-level PM 2.5 concentrations over three megalopolises in China using satellite-derived aerosol optical depth measurements. Atmos. Environ. 124, 232–242.